Micromechanical and fracture behaviors of Ellipsoidal Graphite Reinforced AA2024 Alloy Matrix Composites

A. Chennakesava Reddy

Assistant Professor, Department of Mechanical Engineering, MJ College of Engineering and Technology, Hyderabad, India
dr_acreddy@yahoo.com

Abstract: *A square array unit cell/2-D graphite ellipsoidal particle RVE models were used to evaluate micromechanical behavior and interfacial debonding in AA2024/graphite composites. The particulate metal matrix composites were fabricated from graphite nanoparticles reinforced at different volume fractions in the AA2024 alloy matrix. The heat treated specimens were tensile tested. Interfacial fracture was observed in all the composites.*

Keywords: AA2024*, graphite, ellipsoidal particle, RVE model, finite element analysis, interfacial debonding.*

1. INTRODUCTION

As the mechanical properties of the particulate metal matrix composites are critically determined by the shape, volume fractions, size, and the interactions between the matrix and particles, a detailed understanding of the microstructural property relationships is required for their engineering applications. Some theoretical analysis models have been examined to predict the mechanical properties and determine the micromechanical properties of particle composites [1]. However, these theoretical models were unable to examine the overall elastic-plastic response during the deformation. On the other hand, numerical micromechanical modeling analysis appears to be well-suited to describe the behavior of these composites [2-7]. Currently, the use of a representative volume element (RVE) [8-15] of the composite microstructure, in conjunction with a finite element (FE) analysis tool, is well established for examining the effective material properties and understanding the micromechanics of the composite materials [16].

The objective of this paper is to predict micromechanical properties and interfacial debonding of AA2024/graphite nanoparticle composites using RVE model through finite Element analysis. The results obtained from the finite element analysis were verified with those obtained from the experimentation.

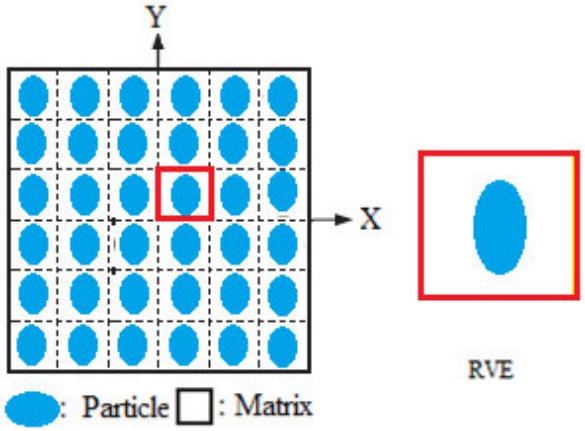

Figure 1: A hexagonal RVE containing an ellipsoidal nanoparticle.

2. THEORETICAL BACKGROUND

To derive the formulae for the equivalent material constants, a homogenized elasticity model of the square representative volume element (RVE) as shown in figure1 is considered. The dimensions of the three-dimensional RVE are $2a$ x $2a$ x $2a$. The cross-sectional area of the RVE is $2a$ x $2a$. The elasticity model is filled with a single, transversely isotropic material that has five independent material constants (elastic moduli E_y and E_z, Poison's ratios v_{xy}, v_{yz} and shear modulus G_{yz}). The general strain-stress relations relating the normal stresses and the normal stains are given below:

$$\varepsilon_x = \frac{\sigma_x}{E_x} - \frac{v_{xy}\sigma_y}{E_y} - \frac{v_{xz}\sigma_z}{E_z} \quad (1)$$

$$\varepsilon_y = -\frac{v_{yx}\sigma_x}{E_y} + \frac{\sigma_y}{E_y} - \frac{v_{yz}\sigma_z}{E_z} \quad (2)$$

$$\varepsilon_z = -\frac{v_{zx}\sigma_x}{E_x} - \frac{v_{zy}\sigma_y}{E_y} + \frac{\sigma_z}{E_z} \quad (3)$$

Let assume that $\sigma_{xy} = \sigma_{yx}, \sigma_{yz} = \sigma_{zy}$ and $\sigma_{zx} = \sigma_{xz}$. For plane strain conditions,$\epsilon_z = 0, \epsilon_{yz} = \varepsilon_{zx} = 0$ and $\varepsilon_{yz} = \varepsilon_{zx}$. The above equations are rewritten as follows:

$$\varepsilon_x = \frac{\sigma_x}{E_x} - \frac{v_{xy}\sigma_y}{E_y} - \frac{v_{yz}\sigma_z}{E_z} \quad (4)$$

$$\varepsilon_y = -\frac{v_{xy}\sigma_x}{E_y} + \frac{\sigma_y}{E_y} - \frac{v_{yz}\sigma_z}{E_z} \quad (5)$$

$$\varepsilon_z = -\frac{v_{yz}\sigma_x}{E_z} - \frac{v_{yz}\sigma_y}{E_z} + \frac{\sigma_z}{E_z} \quad (6)$$

To determine E_y and E_z, v_{xy} and v_{yz}, four equations are required. Two loading cases as shown in figure 2 have been designed to give four such equations based on the theory of elasticity. For load case (figure 2a), the stress and strain components on the lateral surface are:

$$\sigma_x = \sigma_y = 0$$

$$\varepsilon_x = \frac{\Delta a}{a} \text{ along } x = \pm a \text{ and } \varepsilon_y = \frac{\Delta a}{a} \text{ along } y = \pm a$$

$$\varepsilon_z = \frac{\Delta a}{a}$$

where Δa is the change of dimension a of cross-section under the stretch Δa in the z-direction. Integrating and averaging Eq. (6) on the plane z = a, the following equation can be arrived:

$$E_z = \frac{\sigma_{ave}}{\varepsilon_z} = \frac{a}{\Delta a}\sigma_{ave} \quad (7)$$

where the average value of σ_z is given by:

$$\sigma_{ave} = \iint \sigma_z(x, y, a)dxdy \quad (8)$$

The value of σ_{ave} is evaluated for the RVE using finite element analysis (FEA) results.

Using Eq. (5) and the result (7), the strain along $y = \pm a$:

$$\varepsilon_y = -\frac{v_{yz}\sigma_z}{E_z} = -v_{yz}\frac{\Delta a}{a} = \frac{\Delta a}{a}$$

Hence, the expression for the Poisson's ratio v_{yz} is as follows:

$$v_{yz} = -1 \quad (9)$$

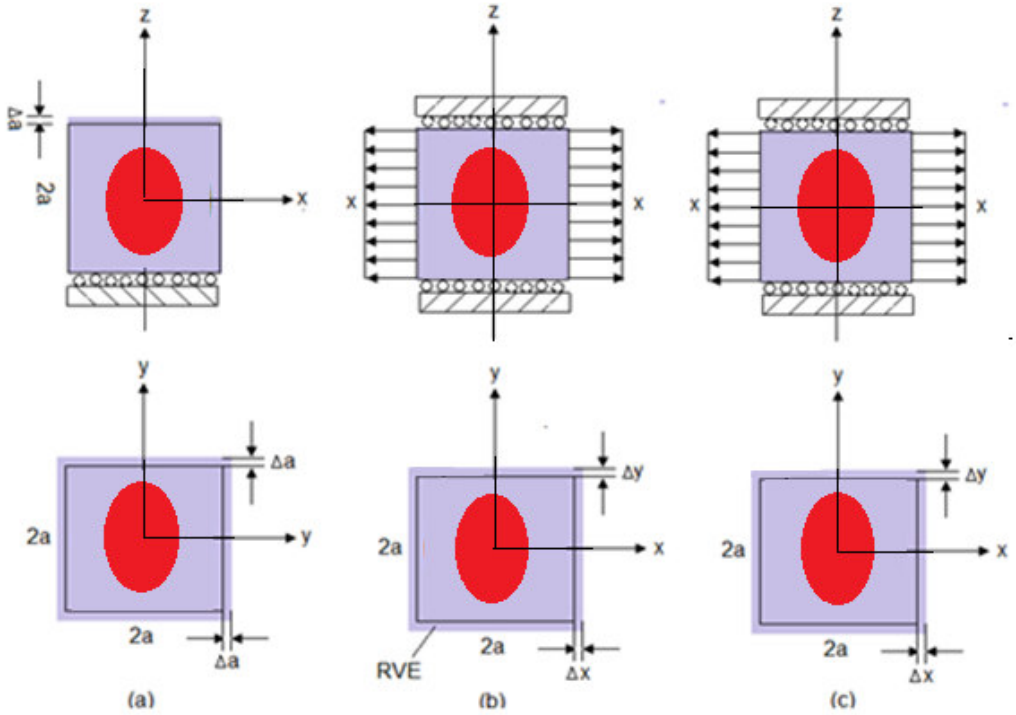

Figure 2: RVE models

For load case (figure 2b), the square representative volume element (RVE) is loaded with a uniformly distributed load (negative pressure), P in a lateral direction, for instance, the x-direction. The RVE is constrained in the z-direction so that the plane

strain condition is sustained to simulate the interactions of RVE with surrounding materials in the z-direction. Since $\varepsilon_z = 0$, $\sigma_z = v_{yz}(\sigma_x + \sigma_y)$ for the plain stress, the strain-stress relations can be reduced as follows:

$$\varepsilon_x = \left(\frac{1}{E_x} - \frac{1}{E_z}\right)\sigma_x - \left(\frac{v_{xy}}{E_y} + \frac{1}{E_z}\right)\sigma_y \quad (10)$$

$$\varepsilon_y = -\left(\frac{v_{xy}}{E_x} + \frac{1}{E_z}\right)\sigma_x + \left(\frac{1}{E_x} - \frac{1}{E_z}\right)\sigma_y \quad (11)$$

For the elasticity model as shown in figure 2b, one can have the following results for the normal stress and strain components at a point on the lateral surface:

$\sigma_y = 0, \sigma_x = P$

$\varepsilon_x = \frac{\Delta x}{a}$ along $x = \pm a$ and $\varepsilon_y = \frac{\Delta y}{a}$ along $y = \pm a$

where Δx (>0) and Δy (<0) are the changes of dimensions in the x- and y- direction, respectively for the load case shown in figure 2b. Applying Eq. (11) for points along $y = \pm a$ and Eq. (10) for points along $x = \pm a$, we get the following:

$$\varepsilon_y = -\left(\frac{v_{xy}}{E_x} + \frac{1}{E_z}\right)P = \frac{\Delta y}{a} \quad (12)$$

$$\varepsilon_x = \left(\frac{1}{E_x} - \frac{1}{E_z}\right)P = \frac{\Delta x}{a} \quad (13)$$

By solving Eqs. (12) and (13), the effective elastic modulus and Poisson's ratio in the transverse direction (xy-plane) as follows:

$$E_x = \frac{1}{\frac{\Delta x}{Pa} + \frac{1}{E_z}} \text{ and } E_y = \frac{1}{\frac{\Delta y}{Pa} + \frac{1}{E_z}} \quad (14)$$

$$v_{xy} = \left(\frac{\Delta y}{Pa} + \frac{1}{E_z}\right)/\left(\frac{\Delta x}{Pa} + \frac{1}{E_z}\right) \quad (15)$$

In which E_z can be determined from Eq. (15). Once the change in lengths along x- and y- direction (Δx and Δy) are determined for the square RVE from the FEA, E_y (= E_x) and v_{xy} can be determined from Eqs. (14) and (15), correspondingly.

The strength of a particulate metal matrix composite depends on the strength of the weakest zone and metallurgical phenomena in it. A new criterion is suggested by the author considering adhesion, formation of precipitates, particle size, agglomeration, voids/porosity, obstacles to the dislocation, and the interfacial reaction of the particle/matrix. The formula for the strength of composite is stated below:

$$\sigma_c = \left[\sigma_m \left\{\frac{1-(v_p+v_v)^{2/3}}{1-1.5(v_p+v_v)}\right\}\right] e^{m_p(v_p+v_v)} + k d_p^{-1/2} \quad (16)$$

$k = E_m m_m / E_p m_p$

where, v_v and v_p are the volume fractions of voids/porosity and nanoparticles in the composite respectively, m_p and m_m are the possion's ratios of the nanoparticles and matrix respectively, d_p is the mean nanoparticle size (diameter) and E_m and E_p is elastic moduli of the matrix and the particle respectively. Elastic modulus (Young's modulus) is a measure of the stiffness of a material and is a quantity used to characterize materials. Elastic modulus is the same in all orientations for isotropic materials. Anisotropy can be seen in many composites. The proposed equations by the author to find Young's modulus of composites and interphase including the effect of voids/porosity as given below:

The upper-bound equation is given by

$$\frac{E_c}{E_m} = \left(\frac{1-v_v^{2/3}}{1-v_v^{2/3}+v_v}\right) + \frac{1+(\delta-1)v_p^{2/3}}{1+(\delta-1)(v_p^{2/3}-v_p)} \quad (17)$$

The lower-bound equation is given by

$$\frac{E_c}{E_m} = 1 + \frac{v_p - v_p}{\delta/(\delta-1)-(v_p+v_v)^{1/3}} \quad (18)$$

where, $\delta = E_p/E_m$.

The transverse modulus is given by

$$E_t = \frac{E_m E_p}{E_m + E_p(1-v_p^{2/3})/v_p^{2/3}} + E_m\left(1 - v_p^{2/3} - v_v^{2/3}\right) \quad (19)$$

3. MATERIALS METHODS

The matrix material was AA2024 aluminum alloy. AA2024 alloy contains copper (4.4%Cu), magnesium (1.5%Mg) and manganese (0.6%Mn) as its major alloying elements. The reinforcement material was ellipsoidal graphite nanoparticles of average size 100nm. The mechanical properties of materials used in the present work are given in table 1.

Table 1: Mechanical properties of AA2024 matrix and graphite nanoparticles

Property	AA2024	graphite
Density, g/cc	2.8	2.51
Elastic modulus, GPa	72.4	445
Ultimate tensile strength, MPa	345	415
Poisson's ratio	0.33	0.19

3.1 Preparation of Composite Specimens

The matrix alloys and composites were prepared by the stir casting and low-pressure die casting process. The volume fractions of graphite reinforcement were 10%, 20%, and 30%. AA2024 matrix alloy was melted in a resistance furnace. The crucibles were made of graphite. The melting losses of the alloy constituents were taken into account while preparing the charge. The charge was fluxed with coverall to prevent dressing. The molten alloy was degasified by tetrachlorethane (in solid form). The crucible was taken away from the furnace; and the melt was treated with sodium modifier. Then the liquid melt was allowed to cool down just below the liquidus temperature to get the melt semi solid state. At this stage, the preheated (500^0C for 1 hour) reinforcement particles and magnesium (Mg) as a wetting agent were added to the liquid melt. The molten alloy and reinforcement particles are thoroughly stirred manually for 15 minutes. After manual steering, the semi-solid, liquid melt was reheated, to a full liquid state in the resistance furnace followed by an automatic mechanical stirring using a mixer to make the melt homogenous for about 10 minutes at 200 rpm. The temperature of melted metal was measured using a dip type thermocouple. The preheated cast iron die was filled with dross-removed melt by the compressed (3.0 bar) argon gas.

3.2 Heat Treatment

Prior to the cold rolling of composite samples, a solution treatment was applied at 535^0C for 1 hour, followed by quenching in cold water. The samples were cold rolled to 2% reduction. In a laboratory mill a relatively low strain rate, probably less than 1. Lubricated rolls were used at maximum speed. The strain was calculated from the thicknesses of the test samples before and after rolling process. The strain measurements are defined by:

$$\varepsilon = ln(t_0/t)$$

$$\varepsilon_{vM} = 2/\sqrt{3}\,\varepsilon \qquad (20)$$

3.2 Tensile Tests

The heat-treated samples were machined to get flat-rectangular specimens (figure 3) for the tensile tests. The tensile specimens were placed in the grips of a Universal Test Machine (UTM) at a specified grip separation and pulled until failure. The test speed was 2 mm/min (as for ASTM D3039). A strain gauge was used to determine elongation.

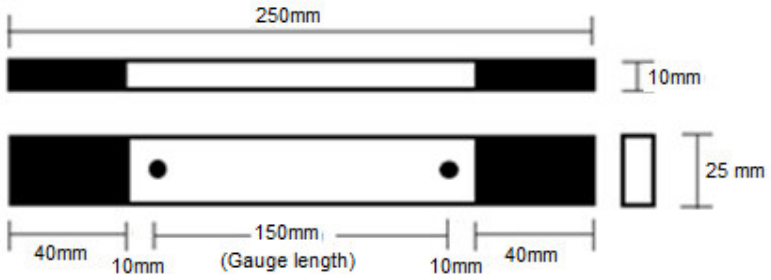

Figure 3: Shape and dimensions of tensile specimen

3.3 Optical and Scanning Electron Microscopic Analysis

An image analyzer was used to study the distribution of the graphite reinforcement particles within the AA2024 matrix. The polished specimens were ringed with distilled water, and etched with a solution (distilled water: 190 ml, nitric acid: 5ml, hydrochloric acid: 3 ml and hydrofluoric acid: 2 ml) for optical microscopic analysis. Fracture surfaces of the deformed/fractured test samples were analyzed with a scanning electron microscope (SEM) to define the macroscopic fracture mode and to establish the microscopic mechanisms governing fracture. Samples for SEM observation were obtained from the tested specimens by sectioning parallel to the fracture surface and the scanning was carried using S-3000N Toshiba SEM.

3.4 **Finite Element Analysis (FEA)**

The representative volume element (RVE or the unit cell) is the smallest volume over which a measurement can be made that will yield a value representative of the whole. In this research, a cubical RVE was implemented to analyze the tensile behavior AA2024/graphite nanoparticle composites. The determination of the RVE's dimensional conditions requires the establishment of a volumetric fraction of ellipsoidal nanoparticles in the composite. Hence, the weight fractions of the particles were converted to volume fractions. The volume fraction of a particle in the RVE is determined:

$$v_p(\text{RVE}) = \frac{\text{Volume of nanoparticle}}{\text{Volume of RVE}} = \frac{16}{3} \times \left(\frac{r}{a}\right)^3 \quad (21)$$

where, r represents the particle radius and a indicates the diameter of the cylindrical RVE. The volume fraction of the particles in the composite (V_p) is obtained using equation

$$Vp = (w_p/\rho_p)/(w_p/\rho_p + w_m/\rho_m) \quad (22)$$

where ρ_m and ρ_p denote the matrix and particle densities, and w_m and w_p indicate the matrix and particle weight fractions, respectively.

The RVE dimension (a) was determined by equalizing Eqs. (21) and (22). The loading on the RVE was defined as symmetric displacement, which provided equal displacements at both ends of the RVE. To obtain the nanocomposite modulus and yield strength, the force reaction was defined against displacement. The large strain PLANE183 element was used in the matrix in all the models. In order to model the adhesion between the matrix and the particle, a CONTACT 172 element was used. For an exact nonlinear solution the converge criteria is also important to set the strain rates of the FEM models based on the experimental tensile tests' setups. Hence, FEM models of different RVEs with various particle contents should have comparable error values. In this respect, the ratio of the tensile test speed to the gauge length of the specimens should be equal to the corresponding ratio in the RVE displacement model.

4. RESULTS AND DISCUSSION

The micromechanical behavior is discussed in terms of tensile elastic moduli, E_x, shear modulus, G_{xy} and major Poisson's ratio, v_{xy}. The fracture behavior is conversed in terms of interface debonding and particle fracture.

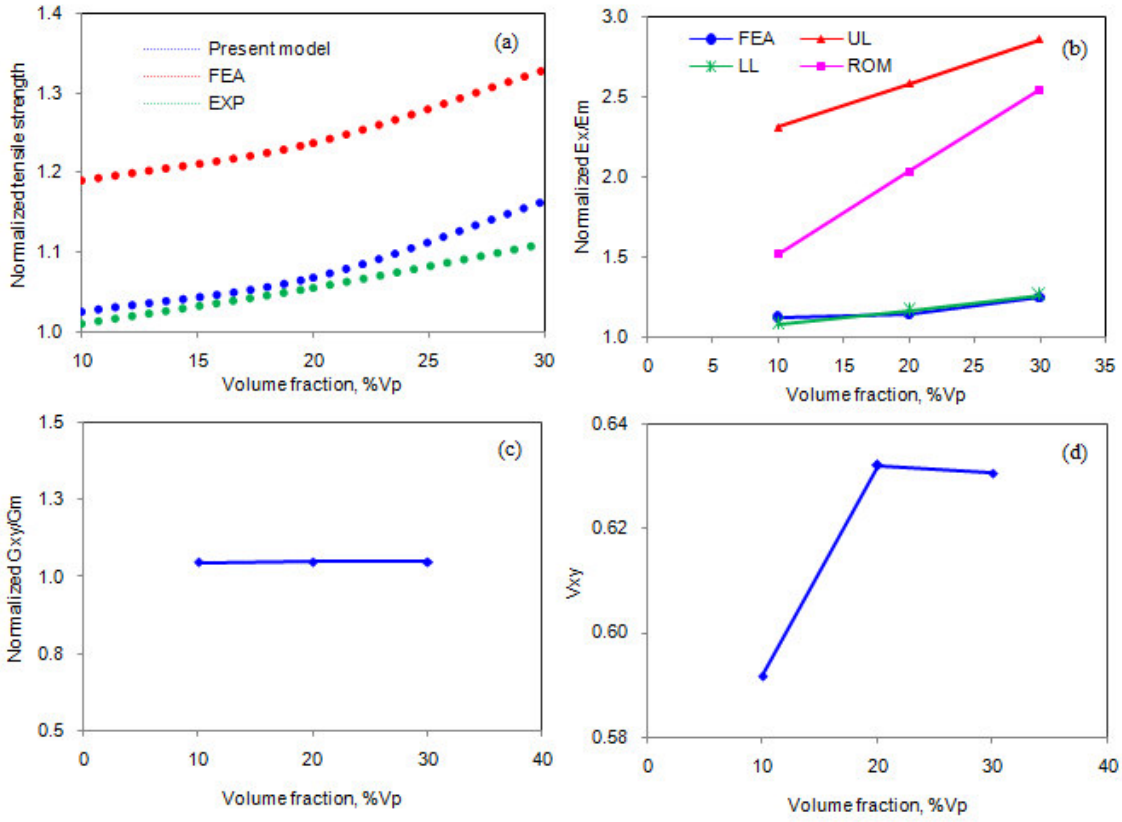

Figure 4: Effect of volume fraction on micromechanical behavior of AA2024/graphite composites.

4.1 Micromechanical Behavior

Figure 4a depicts the normalized tensile strengths of the AA2024/graphite composites obtained by FEA (RVE models), present mathematical model, and experimental procedure. The tensile strength is normalized with ultimate tensile strength of AA2024 alloy matrix. Present mathematical model includes the effect of voids present in the composite. The difference between the FEA results and the experiments results varies from 62 to 75 MPa. This differentiation can be attributed to the presence of voids in the composites, distribution of particles in the matrix, agglomeration of particles and lack of wettability of the particles with the matrix. The difference between the results obtained from present mathematical model and the experimentation varies from 4 to18 MPa. The maximum difference is with high volume fraction of graphite. The difference between the results obtained from present mathematical model and the FEA varies from 56 to58 MPa. The deviation of FEA (RVE model) results with the results computed by the present mathematical model may be as a result of micro-metallurgical factors (such as formation of voids and nanoparticle clustering) that were not considered in the RVE models. However, the nonlinear deformation behavior of the reinforcements and the matrix/reinforcement debonding were considered in the RVE models. These micromechanical factors are important in the large plastic deformation regime. However, the tensile strength increases with increase of volume fraction of graphite in the composite.

The normalized elastic and shear moduli are illustrated in figures 4b and 4c, respectively. The elastic modulus and shear modulus are normalized with the elastic modulus of AA2024 alloy matrix. The stiffness of the composites increases with increase of volume fraction of graphite. The lower limit (LL) values obtained from the present mathematical model coincide with those obtained from FEA. The upper limit (UL) values computed by the present mathematical model are higher than those values obtained by the 'Role of Mixtures (ROM)'and FEA. This is because of consideration of voids in the present mathematical model. The voids improve the stiffness of the composites but reduce the strength of the composites. The shear strength of the composites is enhanced by 5% as compared to that of AA2024 alloy matrix. The major Poisson's ratio increases with increase of volume fraction of graphite particles up to 20% and above this percentage it becomes constant (figure 4d).

4.2 Fracture Analysis

The elastic stress transfer is analyzed by one-dimensional, shear-lag methods. The rate of change of the stress in the particle to the interfacial shear stress at that point and the particle radius, 'r':

$$\frac{d\sigma_p}{dx} = -\frac{\tau_i}{r} \tag{23}$$

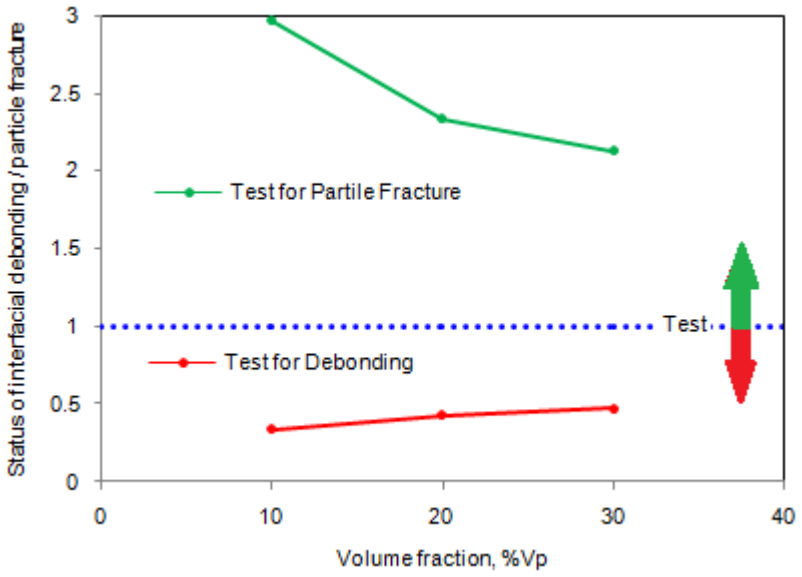

Figure 5: Criterion for particle fracture or interfacial debonding.

If the particle deforms in an elastic manner (according to Hooke's law) then,

$$\tau = \frac{n}{2}\sigma_p \tag{24}$$

where σ_p is the particle stress. If particle fracture occurs when the stress in the particle reaches its ultimate tensile strength, $\sigma_{p,uts}$, then setting the boundary condition at

$$\sigma_p = \sigma_{p,\,uts} \tag{25}$$

The relationship between the strength of the particle and the interfacial shear stress is such that if

$$\sigma_{P,uts} < \frac{2\tau}{n} \quad \text{or} \quad \sigma_{P,uts} / \frac{2\tau}{n} < 1 \tag{26}$$

Then the particle will fracture. From the figure 5, it is observed that the graphite particle is not fractured. The ultimate tensile strength of the graphite nanoparticle is 415 MPa which is higher than the shear stress developed at the interface. Similarly if interfacial debonding/yielding is considered to occur when the interfacial shear stress reaches its shear strength

$$\tau = \tau_{max} \tag{27}$$

For particle/matrix interfacial fracture can be established whereby,

$$\tau_{max} < \frac{n\sigma_p}{2} \quad \text{or} \quad \tau_{max} / \frac{n\sigma_p}{2} < 1 \tag{28}$$

It is observed from figure 5 that the interfacial debonding occurs between graphite nanoparticle and AA2024 alloy matrix as the condition in Eq.(28) is satisfied.

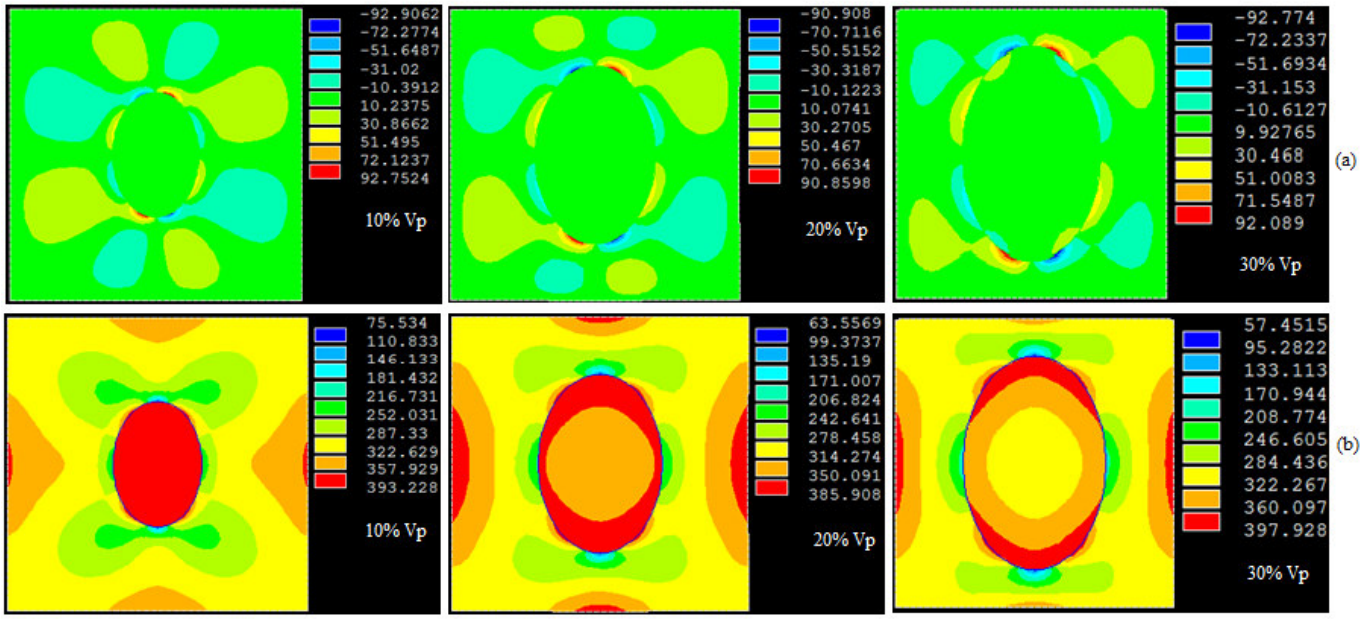

Figure 6: Images obtained from FEA: (a) shear stress and (b) von Mises Stress.

As seen from 6 the shear stress developed at the interfaces are lower than the von Mises stresses induced in the nanoparticle. The von Mises stresses induced around the nanoparticle is much higher than that at the interfaces except in the composites having 10% graphite nanoparticles. The interfacial debonding was high between the particle and the matrix because of local stress concentration around the nanoparticle. The plastic flows were initiated within the matrix and ended at the nanoparticle/matrix interface. Owing to the high stress in the nanoparticles, the plastic deformation becomes concentrated at several locations in the matrix. The localized strain was observed around the particle because of the high load-transfer effect into the particles. The plastic behavior differs considerably with inclusion of interface between the nanoparticle and the matrix.

5. CONCLUSION

The RVE models give the trend of phenomenon happening in the AA2024/graphite composites. The tensile strengths obtained by the mathematical model with voids presented by the author are in good agreement with the experimental results. In the case of composites with perfect adhesion between the nanoparticle and the matrix, the stress is transferred through shear from the matrix to the particles. The tensile strength and elastic modulus increase with an increase volume fraction of graphite nanoparticles in the AA2024 alloy matrix. The interfacial debonding is observed in all the composites.

REFERENCES

1. J. Schroder, K. U. Kainer, Magnesium Base Hybrid Composites Prepared by Liquid state fabrication, Material Science and Engineering, A 135, 1991, pp. 33-36.
2. A. Chennakesava Reddy, Interfacial Debonding Analysis in Terms of Interfacial Tractions for Titanium Boride/AA3003 Alloy Metal Matrix Composites, 1st National Conference on Modern Materials and Manufacturing , Pune, India, 19-20 December 1997, pp. 124-127.

3. A. Chennakesava Reddy, Evaluation of Debonding and Dislocation Occurrences in Rhombus Silicon Nitride Particulate/AA4015 Alloy Metal Matrix Composites, 1st National Conference on Modern Materials and Manufacturing , Pune, India, 19-20 December 1997, pp. 278-282.
4. A. Chennakesava Reddy, Assessment of Debonding and Particulate Fracture Occurrences in Circular Silicon Nitride Particulate/AA5050 Alloy Metal Matrix Composites , National Conference on Materials and Manufacturing Processes, Hyderabad, India, 27-28 February 1998, pp. 104-109.
5. A. Chennakesava Reddy, Local Stress Differential for Particulate Fracture in AA2024/Titanium Carbide Nanoparticulate Metal Matrix Composites, National Conference on Materials and Manufacturing Processes, Hyderabad, India, 27-28 February 1998, pp. 127-131.
6. A. Chennakesava Reddy, Cohesive Zone Finite Element Analysis to Envisage Interface Debonding in AA7020/Titanium Oxide Nanoparticulate Metal Matrix Composites , 2nd International Conference on Composite Materials and Characterization, Nagpur, India, 9-10 April 1999, pp. 204-209.
7. B. Kotiveera Chari, A. Chennakesava Reddy, Interfacial Debonding Analysis in Nanoparticulate Reinforced Metal Matrix Composites of AA8090/Zirconium Carbide, 2nd International Conference on Composite Materials and Characterization, Nagpur, India, 9-10 April 1999, pp. 210-214.
8. H. B. Niranjan, A. Chennakesava Reddy, Debonding Failure and Volume Fraction Effects in Nano-reinforced Composites of AA2024/Silicon Oxide, 2nd International Conference on Composite Materials and Characterization, Nagpur, India, 9-10 April 1999, pp. 215-219.
9. B. Kotiveera Chari, A. Chennakesava Reddy, Effect of Debonding on Overall Behavior of AA3003/Titanium Carbide Nanoparticulate Reinforced Metal Matrix Composites, 2nd International Conference on Composite Materials and Characterization, Nagpur, India, 9-10 April 1999, pp. 220-224.
10. P. M. Jebaraj, A. Chennakesava Reddy, Analysis of Debonding along Interface of AA4015/Magnesium Oxide Nanoparticulate Reinforced Metal Matrix Composites, 2nd International Conference on Composite Materials and Characterization, Nagpur, India, 9-10 April 1999, pp. 225-229.
11. H. B. Niranjan, A. Chennakesava Reddy, Effect of Particulate Debonding in AA5050/Boron Nitride Nanoparticulate Reinforced Metal Matrix Composites, 2nd International Conference on Composite Materials and Characterization, Nagpur, India, 9-10 April 1999, pp. 230-234.
12. P. M. Jebaraj, A. Chennakesava Reddy, Interface Debonding Prediction Technique for Tensile Loaded AA6061/Zirconium Oxide Nanoparticulate MMC, 2nd International Conference on Composite Materials and Characterization, Nagpur, India, 9-10 April 1999, pp. 235-239.
13. S. Sundara Rajan, A. Chennakesava Reddy, FEM Model for Volume Fraction Dependent Interface Debonding in TiN Nanoparticle Reinforced AA7020 Metal Matrix Composites, 2nd International Conference on Composite Materials and Characterization, Nagpur, India, 9-10 April 1999, pp. 240-244.
14. S. Sundara Rajan, A. Chennakesava Reddy, Deformation Behavior of AA8090/ TiO2 Nanoparticulate Reinforced Metal Matrix Composites with Debonding Interfaces, 2nd International Conference on Composite Materials and Characterization, Nagpur, India, 9-10 April 1999, pp. 245-248.
15. A. Chennakesava Reddy, Micromechanical Modelling of Interfacial Debonding in AA1100/Graphite Nanoparticulate Reinforced Metal Matrix Composites, 2nd International Conference on Composite Materials and Characterization, Nagpur, India, 9-10 April 1999, pp. 249-253.
16. Y.J. Liu and X.L. Chen, Evaluations of the effective material properties of carbon nanotube-based composites using a nanoscale representative volume element, Mechanics of Materials, 35, 2003, pp.69–81.